J|A|C|S
ARTICLES
Published on Web 02/02/2007

# Exploring the Subtleties of Drug−Receptor Interactions: The Case of Matrix Metalloproteinases

Ivano Bertini,*[,†,‡] Vito Calderone,[†] Marco Fragai,[†,§] Andrea Giachetti,[†,§,||] Mauro Loconte,[||] Claudio Luchinat,[†,§] Massimiliano Maletta,[†,‡] Cristina Nativi,[⊥] and Kwon Joo Yeo[†]

*Contribution from the Magnetic Resonance Center (CERM), University of Florence, Via L. Sacconi 6, 50019 Sesto Fiorentino, Italy, Department of Chemistry, University of Florence, Via della Lastruccia 3, 50019 Sesto Fiorentino, Italy, Department of Agricultural Biotechnology, University of Florence, Via Maragliano, 75-77, 50144 Florence, Italy, ProtEra S.r.l., Via delle Idee, 22, 50019 Sesto Fiorentino, Italy, and Department of Organic Chemistry, University of Florence, Via della Lastruccia 13, 50019 Sesto Fiorentino, Italy*

Received July 19, 2006; E-mail: ivanobertini@cerm.unifi.it

***Abstract:*** By solving high-resolution crystal structures of a large number (14 in this case) of adducts of matrix metalloproteinase 12 (MMP12) with strong, nanomolar, inhibitors all derived from a single ligand scaffold, it is shown that the energetics of the ligand−protein interactions can be accounted for directly from the structures to a level of detail that allows us to rationalize for the differential binding affinity between pairs of closely related ligands. In each case, variations in binding affinities can be traced back to slight improvements or worsening of specific interactions with the protein of one or more ligand atoms. Isothermal calorimetry measurements show that the binding of this class of MMP inhibitors is largely enthalpy driven, but a favorable entropic contribution is always present. The binding enthalpy of acetohydroxamic acid (AHA), the prototype zinc-binding group in MMP drug discovery, has been also accurately measured. In principle, this research permits the planning of either improved inhibitors, or inhibitors with improved selectivity for one or another MMP. The present analysis is applicable to any drug target for which structural information on adducts with a series of homologous ligands can be obtained, while structural information obtained from *in silico* docking is probably not accurate enough for this type of study.

## Introduction

Drug discovery projects aim at finding small molecules that bind a selected protein target with high binding affinity. High selectivity is also a desirable property especially when the selected target belongs to a protein family. In the case of matrix metalloproteinases (MMP), a family of closely related zinc-containing extracellular proteases, numerous high affinity inhibitors are available.[1] Well-known examples are batimastat and marimastat belonging to the class of succinate peptidomimetic inhibitors,[2,3] the class of succinate macrocyclic inhibitors,[4] the class of sulfone hydroxamate inhibitors,[5] the class of the reverse hydroxamic acid inhibitors,[6] and the class of sulfonamidic inhibitors such as NNGH.[7] Their dissociation constants are in the low nanomolar range. However, the selectivity versus one or another MMP is often modest, and this is at the origin of several side-effects discovered during the clinical trials.[8] Several approaches have been proposed in order to design selective ligands for protein targets.[9−12] Three-dimensional structures of enzyme−inhibitor adducts for several ligands, belonging to the various classes, with several different MMPs are available.[3,5,13−22]

[†] Magnetic Resonance Center (CERM), University of Florence.
[‡] Department of Chemistry, University of Florence.
[§] Department of Agricultural Biotechnology, University of Florence.
[||] ProtEra S.r.l.
[⊥] Department of Organic Chemistry, University of Florence.

(1) Fisher, J. F.; Mobashery, S. *Cancer Metastasis Rev.* **2006**, *25*, 115−136.
(2) Whittaker, M.; Floyd, C. D.; Brown, P.; Gearing, A. J. *Chem. Rev.* **1999**, *99*, 2735−2776.
(3) Skiles, J. W.; Gonnella, N. C.; Jeng, A. Y. *Curr. Med. Chem.* **2004**, *11*, 2911−2977.
(4) Xue, C. B.; He, X. H.; Corbett, R. L.; Roderick, J.; Wasserman, Z. R.; Liu, R. Q.; Jaffee, B. D.; Covington, M. B.; Qian, M. X.; Trzaskos, J. M.; Newton, R. C.; Magolda, R. L.; Wexler, R. R.; Decicco, C. P. *J. Med. Chem.* **2001**, *44*, 3351−3354.
(5) Lovejoy, B.; Welch, A. R.; Carr, S.; Luong, C.; Broka, C.; Hendricks, R. T.; Campbell, J. A.; Walker, K. A. M.; Martin, R.; Van Wart, H.; Browner, M. F. *Nat. Struct. Biol.* **1999**, *6*, 217−221.
(6) Hajduk, P. J. et al. *J. Am. Chem. Soc.* **1997**, *119*, 5818−5827.
(7) MacPherson, L. J. et al. *J. Med. Chem.* **1997**, *40*, 2525−2532.
(8) Coussens, L. M.; Fingleton, B.; Matrisian, L. M. *Science* **2002**, *295*, 2387−2392.
(9) Johnson S. L.; Pellecchia M. *Curr. Top. Med. Chem.* **2006**, *6*, 317−329.
(10) Zartler, E. R.; Shapiro, M. J. *Curr. Opin. Chem. Biol.* **2005**, *9*, 366−370.
(11) Erlanson, D. A.; Wells, J. A.; Braisted, A. C. *Annu. Rev. Biophys. Biomol. Struct.* **2004**, *33*, 199−223.
(12) Blundell, T. L.; Jhoti, H.; Abell, C. *Nat. Rev. Drug Discovery* **2002**, *1*, 45−54.
(13) Moy, F. J.; Chanda, P. K.; Chen, J. M.; Cosmi, S.; Edris, W.; Levin, J. I.; Powers, R. *J. Mol. Biol.* **2000**, *302*, 671−689.
(14) Brandstetter, H.; Grams, F.; Glitz, D.; Lang, A.; Huber, R.; Bode, W.; Krell, H. W.; Engh, R. A. *J. Biol. Chem.* **2001**, *276*, 17405−17412.
(15) Gall, A. L.; Ruff, M.; Kannan, R.; Cuniasse, P.; Yiotakis, A.; Dive, V.; Rio, M. C.; Basset, P.; Moras, D. *J. Mol. Biol.* **2001**, *307*, 577−586.
(16) Borkakoti, N.; Winkler, F. K.; Williams, D. H.; Darcy, A.; Broadhurst, M. J.; Brown, P. A.; Johnson, W. H.; Murray, E. J. *Nat. Struct. Biol.* **1994**, *1*, 106−110.
(17) Bertini, I.; Calderone, V.; Cosenza, M.; Fragai, M.; Lee, Y.-M.; Luchinat, C.; Mangani, S.; Terni, B.; Turano, P. *Proc. Natl. Acad. Sci. U.S.A* **2005**, *102*, 5334−5339.
(18) Lang, R.; Kocourek, A.; Braun, M.; Tschesche, H.; Huber, R.; Bode, W.; Maskos, K. *J. Mol. Biol.* **2001**, *312*, 731−742.

 **10.1021/ja065156z CCC: $37.00** 

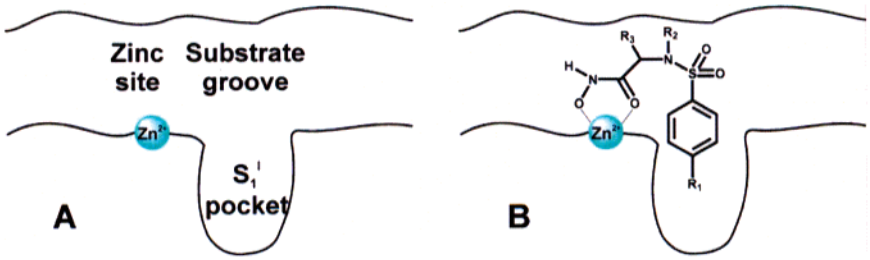


***Figure 1.*** (A) Schematic representation of the active site of MMPs highlighting the zinc ion site, the hydrophobic pocket termed $S_{1'}$, and the substrate binding groove. (B) The sulfonamide scaffold used in this work with its $R_1$, $R_2$ and $R_3$ substituents. The actual compounds investigated are: **1** $R_1 = H$, $R_2 = H$, $R_3 = H$, **2** $R_1 = F$, $R_2 = H$, $R_3 = H$, **3** $R_1 = OCH_3$, $R_2 = H$, $R_3 = H$, **4** $R_1 = C_6H_5$, $R_2 = H$, $R_3 = H$, **5** $R_1 = F$, $R_2 = CH_2CH_2OH$, $R_3 = H$, **6** $R_1 = OCH_3$, $R_2 = CH_2CH_2OH$, $R_3 = H$, **7** $R_1 = C_6H_5$, $R_2 = CH_2CH_2OH$, $R_3 = H$, **8** $R_1 = OCH_3$, $R_2 = H$, $R_3 = (D)CH_2OH$, **9** $R_1 = OCH_3$, $R_2 = H$, $R_3 = (D)CHCH_3OH$, **10** $R_1 = OCH_3$, $R_2 = H$, $R_3 = (L)CH_2OH$, **11** $R_1 = OCH_3$, $R_2 = H$, $R_3 = (L)CHCH_3OH$, **12** $R_1 = OCH_3$, $R_2 = CH_2CH(CH_3)_2$, $R_3 = H$, **13** $R_1 = OCH_3$, $R_2 = CH_2CHOHCH_2OH$, $R_3 = H$, **14** $R_1 = OCH_3$, $R_2 = CH_2CHOHCH_2OH$, $R_3 = (D)CH_2OH$.

Given the active site topology of MMPs, most inhibitors share similar features, i.e., the ability to bind to the metal ion, to the hydrophobic pocket termed $S_1'$, and to the substrate binding groove (Figure 1A). In such a situation, to attempt planning ligands with increased selectivity requires an understanding of the energetics of the inhibitor interactions with each of these active site regions to an unprecedented level of detail. The existing structural data for various MMP−inhibitor adducts are many but scattered, and structure−affinity relationships at the level of a meaningful dissection of the various contributions can be hardly attempted.[23] Furthermore, the catalytic domains of MMPs undergo non-negligible conformational equilibria in solution,[17,24,25] which also involve the active site pocket. A flexible active site is a serious drawback for the use of *in silico* docking programs to design inhibitors,[26] and even more to refine them to increase selectivity.[27]

With this in mind, we felt it would be important to ascertain whether, in case a large number of structures of MMP adducts with a homologous series of ligands were available, structure−affinity relationships can be established, and, if so, whether these relationships are accurate enough to enable meaningful protein-specific ligand-refinement strategies. Thus, we collected structural data for a large number of adducts of a homologous series of ligands with one particular MMP. We selected MMP12, a validated target for emphysema[28] and multiple sclerosis,[29] because a crystalline form of its catalytic domain is available[17] that allows easy soaking of inhibitors. High-resolution crystal structures of as many as 16 different adducts of the protein with structurally related inhibitors were obtained. In parallel, the free energies of binding ($\Delta G^\circ$) through enzyme activity inhibition experiments were measured for the same ligands. It is shown that, indeed, a careful analysis of the structural data, performed with the aid of structure-based computed interatomic interaction energies, can provide a detailed description of how different substituents on the same scaffold can interplay to improve or worsen affinity and selectivity. It is proposed that this strategy is of general validity for any drug target, provided structural information on a number of homologous ligand−protein adducts can be obtained. In particular, other therapeutically relevant metalloproteinases[9,30] may benefit from this approach.

## Materials and Methods

Synthesis, characterization, and inhibitory assays of compounds **1**−**11**, **13**, and **14** will be described elsewhere. Compound **12** has been already described.[7]

**Expression and Purification of Human MMP12 and MMP13 Catalytic Domain.** Cloning, expression, and purification of MMP12 catalytic domain have been previously described.[17] The cDNA of proMMP13 (Leu20-Pro268) was cloned into the pET21 vector (Novagen) using *Nde I* and *Xho I* as restriction enzymes. One additional methionine at position 19 was present in the final expression product. The *E. coli* strain BL21 Codon Plus cells, transformed with the above plasmid, were grown in LB medium at 310 K. The protein expression was induced during the exponential growth phase with 0.5 mM of IPTG. The cells were harvested 3 h after induction. After lysis of the cells, the inclusion bodies, containing the proMMP13, were solubilized in 6 M urea and 20 mM Tris (pH 8.0). The protein was purified on the Hitrap Q column (Pharmacia) with a buffer containing 6 M urea and 20 mM Tris (pH 8.0). The elution was performed using a linear gradient of NaCl up to 0.6 M. The purified protein was then refolded using multistep dialysis against solutions containing 50 mM Tris (pH 7.2), 10 mM $CaCl_2$, 0.1 mM $ZnCl_2$, and 0.3 M NaCl and decreasing concentration of urea. The refolded protein was exchanged, by dialysis, against a buffer with 50 mM Tris (pH 7.2), 5 mM $CaCl_2$, 0.1 mM $ZnCl_2$, and 0.3 M NaCl. The protein was concentrated at room-temperature using an Amicon up to a concentration of about 30 $\mu$M. The active protein is left overnight in these conditions to allow the autoproteolysis of the prodomain. After addition of acetohydroxamic acid (AHA) to a final concentration of 0.5 M, the catalytic domain of MMP13 (Tyr104-Pro268) was purified using size-exclusion chromatography with the buffer containing 50 mM Tris (pH 7.2), 5 mM $CaCl_2$, 0.1 mM $ZnCl_2$, 0.3 M NaCl, and 0.2 M AHA and then concentrated using a Centriprep concentrator at 277 K to a final concentration of 0.3 mM.

(19) Bertini, I.; Calderone, V.; Fragai, M.; Luchinat, C.; Mangani, S.; Terni, B. *J. Mol. Biol.* **2004**, *336*, 707−716.
(20) Vandoren, S. R.; Kurochkin, A. V.; Hu, W. D.; Ye, Q. Z.; Johnson, L. L.; Hupe, D. J.; Zuiderweg, E. R. P. *Protein Sci.* **1995**, *4*, 2487−2498.
(21) Browner, M. F.; Smith, W. W.; Castelhano, A. L. *Biochemistry* **1995**, *34*, 6602−6610.
(22) Rowsell, S.; Hawtin, P.; Minshull, C. A.; Jepson, H.; Brockbank, S. M. V.; Barratt, D. G.; Slater, A. M.; McPheat, W. L.; Waterson, D.; Henney, A. M.; Pauptit, R. A. *J. Mol. Biol.* **2002**, *319*, 173−181.
(23) Rush, T. S.; Powers, R. The Application of X-Ray, NMR, and Molecular Modeling in the Design of MMP Inhibitors. *Curr. Top. Med. Chem.* **2004**, *4*, 1311−1327.
(24) Moy, F. J.; Pisano, M. R.; Chanda, P. K.; Urbano, C.; Killar, L. M.; Sung, M. L.; Powers, R. *J. Biomol. NMR* **1997**, *10*, 9−19.
(25) Gao, G.; Semenchenko, V.; Arumugam, S.; Van Doren, S. R. *J. Mol. Biol.* **2000**, *301*, 537−552.
(26) Teague, S. J. *Nature Rev. Drug Discovery* **2003**, *2*, 527−541.
(27) Moy, F. J.; Chanda, P. K.; Chen, J.; Cosmi, S.; Edris, W.; Levin, J. I.; Rush, T. S.; Wilhelm, J.; Powers, R. *J. Am. Chem. Soc.* **2002**, *124*, 12658−12659.
(28) Morris, D. G.; Huang, X. Z.; Kaminski, N.; Wang, Y. N.; Shapiro, S. D.; Dolganov, G. Glick, A.; Sheppard, D. Nature 2003, 422, 169−173.
(29) Vos, C. M. P.; van Haastert, E. S.; de Groot, C. J. A.; van der Valk, P.; de Vries, H. E. Matrix Metalloproteinase-12 *J. Neuroimmunol.* **2003**, *138*, 106−114.
(30) Forino, M.; Johnson, S.; Wong, T. Y.; Rozanov, D. V.; Savinov, A. Y.; Li, W.; Fattorusso, R.; Becattini, B.; Orry, A. J.; Jung, D. W.; Abagyan, R. A.; Smith, J. W.; Alibek, K.; Liddington, R. C.; Strongin, A. Y.; Pellecchia, M. *Proc. Natl. Acad. Sci. U.S.A.* **2005**, *102*, 9499−9504.

**Fluorimetric Assays.** The inhibition constants for the compounds here investigated were determined, evaluating their ability to prevent the hydrolysis of the fluorescent-quenched peptide substrate Mca-Pro-Leu-Gly-Leu-Dpa-Ala-Arg-$NH_2$ (Biomol Inc.). All measurements were performed in 50 mM HEPES buffer, with 10 mM $CaCl_2$, 0.05% Brij-35, and 0.1 mM $ZnCl_2$ (pH 7.0), using 1 nM enzyme and 1 $\mu$M peptide at 298 K.

**Crystallization, Data Collection, and Resolution of the Crystal Structures.** Crystals of human MMP12, already containing AHA from the refolding process, grew at 293 K from a 0.1 M Tris-HCl/30% PEG 8000/200 mM AHA/1.0 M $LiCl_2$ solution at pH 8.0 using the vapor diffusion technique. The final protein concentration was about 10 mg/mL.

The complexes were obtained through soaking MMP12-AHA crystals with a solution containing the inhibitor itself in the presence of $LiCl_2$. Crystals of MMP12-AHA were obtained in the presence of $LiCl_2$ as well.[17]

The data were measured in-house, using a PX-Ultra copper sealed tube source (Oxford Diffraction), for **3**, **6**, **7**, **9**, **13**, and **14**, at ID29 ESRF (Grenoble, France) for **4** and **8**, at BW7A DESY (Hamburg, Germany) for **1**, **2**, **5**, **10**, and **11** complexes, and at XRD-1 ELETTRA (Trieste, Italy) for **12**. All the datasets were collected at 100 K, and the crystals used for data collection were cryocooled without any cryoprotectant treatment. The crystals of all complexes had a mosaicity ranging from 0.3° to 0.8° and diffracted to a maximum resolution of 1.1 Å.

All the soaked adducts crystallize in the *C*2 space group with one molecule in the asymmetric unit while cocrystallized complex of **12** crystallizes in $P2_12_12$ space group with one molecule in the asymmetric unit.

The data were processed in all cases using the program MOSFLM[31] and scaled using the program SCALA[32] with the TAILS and SECONDARY corrections on (the latter restrained with a TIE SURFACE command) to achieve an empirical absorption correction. Table 1S (in Supporting Information) shows the data collection and processing statistics for all datasets.

The structure of the adduct with **12** was previously solved[17] using the molecular replacement technique; the model used was that of a molecule of human MMP12 (1OS9) while the structure of all other adducts were solved using the MMP12−AHA adduct (1Y93) as the model from where the inhibitor, all the water molecules, and ions were omitted. The correct orientation and translation of the molecule within the crystallographic unit cell was determined with standard Patterson search techniques[33,34] as implemented in the program MOLREP.[35,36] The refinement was carried out using REFMAC5,[37] and for the atomic resolution datasets anisotropic B-factors were also refined. In between the refinement cycles the models were subjected to manual rebuilding by using XtalView.[38] The same program has been used to model all inhibitors. Water molecules have been added by using the standard procedures within the ARP/wARP suite,[39] and for the atomic resolution datasets, hydrogens were added at the riding positions and refined.

The stereochemical quality of the refined models was assessed using the program Procheck.[40] The Ramachandran plot for all structures is of very good quality.

The coordinates for all adducts are under deposition at the Protein-DataBank.

**Energy Calculation.** Autodock 3.05 was used to calculate the protein ligand binding energy.[41] The calculation was performed starting from the X-ray crystal structure using reliable Zn(II) parameters.[42] A box of $70 \times 70 \times 70$ points with grid spacing of 0.375 Å was created on the protein side and centered near the catalytic Zn(II) ion. The ligands were extracted from the X-ray structure, and hydrogen atoms were added considering the hydroxamic group deprotonated; Gaister-Marsili partial atomic charges were calculated using BABEL.[43] The ligands were modeled based on the X-ray structures which were already minimized against the experimental diffraction data. Energy contributions for individual atoms were extracted from the Autodock energy output.

**Calorimetry.** Isothermal Titration Microcalorimetry experiments were performed at 298 K with a VP-ITC microcalorimeter (MicroCal, Inc., Northampton, MA). After an initial injection of 1 $\mu$L, aliquots of 9 $\mu$L of 200 $\mu$M inhibitor were stepwise injected into the sample cell containing a solution 20 $\mu$M of MMP12 catalytic domain until complete saturation. All experiments were performed in 20 mM Tris (pH 7.2), 5 mM $CaCl_2$, 0.1 mM $ZnCl_2$, 0.3 M NaCl, and 4 mM AHA with 0.1% (v/v) DMSO. Heats of dilution were measured by injecting the ligand into buffer and then subtracted from the binding heats. The thermodynamic parameters and $K_A$ values were calculated fitting data to a single binding site model with ORIGIN 7.0 sofware (Microcal, Inc.).[44]

## Results and Discussion

**Crystal Structures and Dissociation Constants of Ligand−MMP12 Adducts.** The crystal structures of the complexes of the catalytic domain of MMP12 with 14 closely related inhibitors have been solved. Figure 1B shows the scaffold common to all these inhibitors, and the three positions on which different functionalizations have been tested. The general formula contains a hydroxamic group targeted to bind the catalytic zinc ion, and an aromatic moiety bearing the $R_1$ substituent targeted to the hydrophobic $S_{1'}$ pocket. The two groups are tethered by a sulfonamide moiety interacting with the substrate binding groove and containing substituents $R_2$ and $R_3$, potentially able to give rise to further interactions. $R_1$ ranges from H to F to $OCH_3$ to $C_6H_5$. These variations were planned to monitor their relative effects on the strength of the interaction with $S_1'$. $R_2$ and $R_3$ are either H or aliphatic groups with various degrees of hydrophobicity/hydrophilicity.

A close up of the arrangement of the various ligands in the active site of MMP12 is shown in Figures 2−6. All the inhibitors share the same binding mode, as expected, and in a first inspection all relevant interactions (with the $S_1'$ pocket, the metal, and the substrate binding groove) are in place. To emphasize the similarities, all structures are reported with the same orientation, obtained by least-square fits of all the coordinates of the adducts to one another. The left-hand column of Figures 2−6 shows the structures of each adduct, and the central column reports the structure of the adduct with the closest ligand homologue.

Despite the similarities of the ligand-protein interactions, the dissociation constants, measured as inhibition constants through fluorimetry under non-saturating substrate concentration condi-

(31) Leslie, A. G. W. In Crystallographic Computing V. In *Molecular Data Processing*; Moras, D.; Podjarny, A. D.; Thierry, J.-C., Eds.; Oxford University Press: Oxford, 1991.
(32) Evans, P. R. Data Reduction. *Proceedings of CCP4 Study Weekend. Data Collection & Processing*; Sawyer, L., Isaacs, N., Bailey, S., Eds.; SERC Daresbury Laboratory: England, 1993; pp 114−122.
(33) Rossmann, M. G.; Blow, D. M. *Acta Crystallogr.* **1962**, *D15*, 24−31.
(34) Crowther, R. A. *The Molecular Replacement Method*; Rossmann, M. G., Ed.; Gordon & Breach: New York, 1972.
(35) Vagin, A.; Teplyakov, A. *J. App. Crystallogr.* **1997**, *30*, 1022−1025.
(36) Vagin, A.; Teplyakov, A. *Acta Crystallogr. D Biol. Crystallogr.* **2000**, *56 Pt 12*, 1622−1624.
(37) Murshudov, G. N.; Vagin, A. A.; Dodson, E. J. *Acta Crystallogr.* **1997**, *D53*, 240−255.
(38) McRee, D. E. *J. Mol. Graphics* **1992**, *10*, 44−47.
(39) Lamzin, V. S. *Acta Crystallogr. D Biol. Crystallogr.* **1993**, *49*, 129−147.
(40) Laskowski, R. A.; MacArthur, M. W.; Moss, D. S.; Thornton, J. M. *J. Appl. Crystallogr.* **1993**, *26*, 283−291.
(41) Morris, G. M.; Goodsell, D. S.; Halliday, R. S.; Huey, R.; Hart, W. E.; Belew, R. K.; Olson, A. J. *J. Comput. Chem.* **1998**, *19*, 1639−1662.
(42) Hu, X.; Shelver, W. H. *J. Mol. Graph. Model.* **2003**, *22*, 115−126.
(43) Shah, A. V.; Walters, W. P.; Shah, R.; Dolata, D. P. *Babel - A molecular Structure Information Interchange Hub*; Lysakowski, R., Gragg, C. E., Eds.; American Society for Testing and Materials: Philadelphia, PA, 1994.
(44) Indyk, L.; Fisher, H. F. *Methods Enzymol.* **1998**, *295*, 350−364.

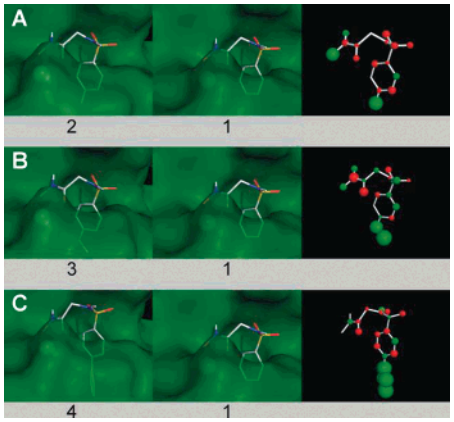


***Figure 2.*** Close up of the high-resolution 3D structures of the adducts of MMP12 with ligands **2**−**4** (left-hand column) and **1** (central column, panels A−C). The right-hand column highlights the improvement (green spheres) and worsening (red spheres) of the protein interaction with individual atoms of ligands **2**−**4** with respect to **1**. The volumes of the spheres are proportional to the size of the interaction energy variation.

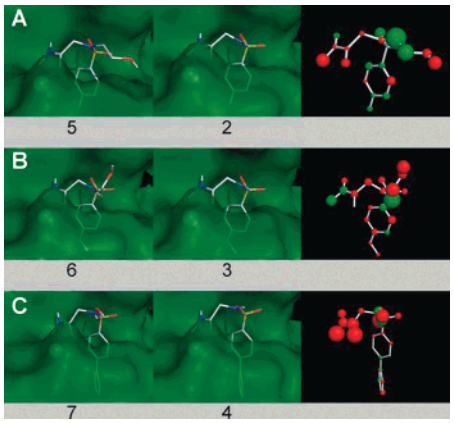


***Figure 3.*** Close up of the high-resolution 3D structures of the adducts of MMP12 with ligands **5**−**7** (left-hand column panels A−C) and **2**−**4** (central column, panels A−C). The right-hand column highlights the improvement (green spheres) and worsening (red spheres) of the protein interaction with individual atoms of ligands **5**−**7** with respect to **2**−**4**, respectively. The volumes of the spheres are proportional to the size of the interaction energy variation.

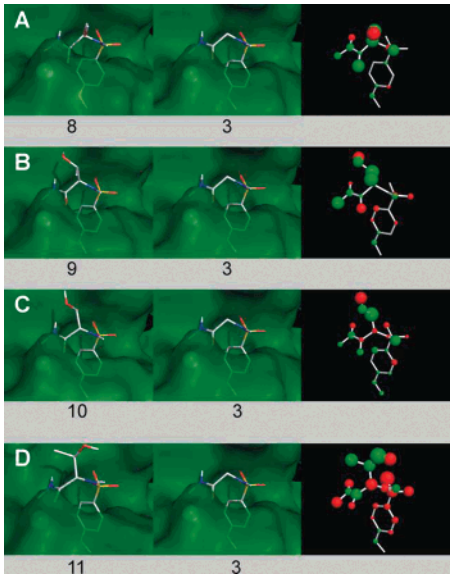


***Figure 4.*** Close up of the high-resolution 3D structures of the adducts of MMP12 with ligands **8**−**11** (left-hand column panels A−D) and **3** (central column, panels A−D). The right-hand column highlights the improvement (green spheres) and worsening (red spheres) of the protein interaction with individual atoms of ligands **8**−**11** with respect to **3**. The volumes of the spheres are proportional to the size of the interaction energy variation.

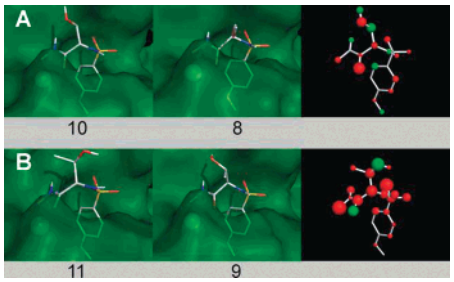


***Figure 5.*** Close up of the high-resolution 3D structures of the adducts of MMP12 with ligands **10** and **11** (left-hand column panels A,B) and **8** and **9** (central column, panels A,B). The right-hand column highlights the improvement (green spheres) and worsening (red spheres) of the protein interaction with individual atoms of ligands **10** and **11** with respect to **8** and **9**. The volumes of the spheres are proportional to the size of the interaction energy variation.

tions at 298 K (see materials and methods), span 2 orders of magnitude. The associated $\Delta G°$ values are reported in Table 1. As described in Materials and Methods, the protein was used as an adduct with the weak inhibitor acetohydroxamic acid (AHA). Stock protein solutions contained 200 mM AHA. At the final dilution for the fluorimetric assays (1 nM enzyme), the AHA concentration was 5 $\mu$M at most, which is well below the dissociation constant of 6.2 mM estimated through the same fluorimetric assay. Therefore, it may be concluded that AHA does not appreciably interfere with the assays. It can be seen that there are relevant differences in binding affinities even between ligands that are very close homologues, i.e., that are next to one another in Figures 2−6.

These results illustrate well the nature of the problem: as large differences in the binding modes can be immediately ruled out by visual inspection, the point is to ascertain whether small differences in the binding mode are at all detectable (the nominal resolution for the adduct structures obtained in this work range between 1.2 and 1.7 Å, which corresponds to indeterminations in interatomic distances of ±0.10 to ±0.15 Å) and, if so, whether these small differences are consistently related with the differences in binding affinity.

Careful examination of key interatomic distances and angles does suggest that indeed not all interactions, despite being all in place, may be energetically equivalent. For example, on passing from $R_1$ = -H (**1**) to $R_1$ = -F (**2**), -$OCH_3$ (**3**), -$C_6H_5$ (**4**), Van der Waals contacts are of course gained in the $S_1'$ pocket, but less optimal H-bond interactions of the $SO_2$ group are seen in all cases. A slight worsening is apparent in the hydroxamic acid coordination mode in the -$OCH_3$ derivative, and a less deep penetration of the first phenyl ring in the $S_1'$ pocket is seen in the -$C_6H_5$ derivative. As another example, by comparing the $R_1$ = -$C_6H_5$, $R_2$ = -$CH_2CH_2OH$, $R_3$ = -H derivative (**7**) with the $R_1$ = -$C_6H_5$, $R_2$ = -H, $R_3$ = -H derivative (**4**) on one side, and the $R_1$ = -$OCH_3$, $R_2$ = -$CH_2CH_2OH$, $R_3$ = -H derivative (**6**) with the $R_1$ = -$OCH_3$, $R_2$ = -H, $R_3$ = -H derivative (**3**) on the other side, we notice that the addition of the $R_2$ = -$CH_2CH_2OH$ substituent may have opposite effects: it modestly improves the overall binding of the $R_1$ = -$OCH_3$ compound and strongly worsens the binding of the $R_1$ = -$C_6H_5$

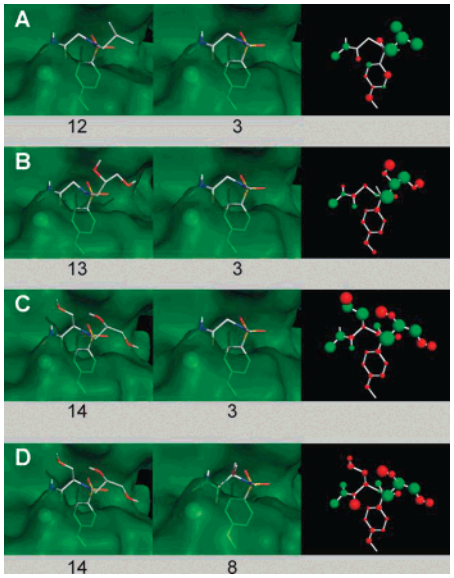


***Figure 6.*** Close up of the high-resolution 3D structures of the adducts of MMP12 with ligands **12**−**14** (left-hand column panels A−D), and **3** (central column, panels A−C), and **8** (central column, panels D). The right-hand column highlights the improvement (green spheres) and worsening (red spheres) of the protein interaction with individual atoms of ligands **12**−**14** with respect to **3** and **14** with respect to **8**. The volumes of the spheres are proportional to the size of the interaction energy variation.

***Table 1.*** Corrected Thermodynamic Parameters for the Investigated Inhibitors

| | $K_D$ (nM) | $\Delta G°$ (kcal/mol) | $\Delta H°$ (kcal/mol) | $-T\Delta S°$ (kcal/mol) |
|---|---|---|---|---|
| **1** | 61.1 | −9.83 | −9.09 | −0.74 |
| **2** | 65.1 | −9.80 | −6.77 | −3.03 |
| **3** | 19.7 | −10.50 | −8.52 | −1.98 |
| **4** | 2.36 | −11.76 | −8.85 | −2.91 |
| **5** | 39.5 | −10.09 | −6.46 | −3.63 |
| **6** | 7.88 | −11.05 | −9.65 | −1.40 |
| **7** | 30.6 | −10.24 | − | − |
| **8** | 5.91 | −11.22 | −8.39 | −2.83 |
| **9** | 10.8 | −10.86 | −8.12 | −2.74 |
| **10** | 41.5 | −10.06 | − | − |
| **11** | 1980 | −7.77 | − | − |
| **12** | 4.20 | −11.42 | −8.24 | −3.18 |
| **13** | 7.88 | −11.05 | −8.89 | −2.16 |
| **14** | 41.5 | −11.12 | −8.08 | −3.04 |
| AHA | $6.18 \times 10^6$ | −3.01 | −3.18 | 0.17 |
| galardin | 7.88 | −11.05 | −4.07 | −6.98 |
| actinonin | 102 | −9.53 | 2.20 | −11.73 |

compound. Inspection of the structures suggests that the worsening of the affinity of the $-C_6H_5$ derivative may be qualitatively explained by the less optimal binding mode of the hydroxamic moiety, with an average distance between the two oxygens being 0.03 Å longer, respectively, in the $-C_6H_5$ with respect to the $-OCH_3$ case. While an increase in binding affinity upon increasing the size of the $R_1$ substituent in the first example could have been expected, the reversal in behavior of the $R_2 = -CH_2CH_2OH$ substitution between the $-OCH_3$ and the $-C_6H_5$ derivatives was unexpected.

**Differential Interaction Energies of Homologous Ligand Pairs.** From careful inspection of the structures, a qualitative correlation seems to exist between good intermolecular interactions and binding affinity. It is difficult, however, to extend these considerations to all molecules, especially when some interactions seem to have improved and other to have been worsened in the same adduct. In other words, it would be desirable to have a simpler but reliable way to translate these observations to contributions to binding. As the individual interaction strengths can be ultimately traced down to either hydrophobic or electrostatic effects, we decided to simply evaluate the hydrophobic and electrostatic contributions to the overall intermolecular interaction energy *by each ligand atom* using standard parameter sets such as those employed in popular docking programs. Among them, the parameter set used by Autodock was selected because of its simple *ad hoc* treatment of the ligand metal ion interaction.[45] It should be immediately stressed that we are not using these parameters to estimate overall, absolute binding energies (see however later) but only to attach a more quantitative meaning to structural observations by calculating *differences* in interatomic interaction energies between the protein and each atom of different homologous ligands. By estimating differences, possible biases originating from crude approximations, for instance those used by Autodock to parametrize the strength of the zinc−hydroxamic ligand coordination bonds, should largely cancel. Furthermore, the differences are taken between ligands that are very close homologues, i.e., are next to one another in Figures 2−6.

The results are reported in pictorial form on the right-hand columns of Figures 2−6. For each row in these figures, the ligand forming the adduct reported in the left-hand side of the figure is drawn, and its atoms are color- and size-coded to show whether their individual interactions with the protein are stronger (green) or weaker (red), and by how much (sphere volume), with respect to those of the corresponding atoms in the central column adduct. For ligand atoms that do not have a corresponding atom in the homologue compound, their interaction strengths with the protein are encoded as such. The right-hand columns of Figures 2−6 thus provide an immediate perception of which atoms may be relevant in determining the differences in affinity when the structures of closely related ligands are compared. We have checked that the results of the above procedure are largely independent of the set of parameters used, suggesting that the estimated differences in interaction energies are reliable. A better way to check their reliability is of course to compare the algebraic sum of all the differences with the difference in experimental $\Delta G°$ values ($\Delta\Delta G°$). This comparison is reported in Figure 7. Remarkably, not only are the signs of the $\Delta\Delta G°$s predicted correctly in most cases, but their magnitudes are also reproduced quite well. In only two cases (**2-1** and **10-3**) is the calculated sign opposite to the predicted one, but in both cases the differences are rather close to zero. An entropic penalty may be further added to the algebraic sum of the individual energetic terms if, between the two ligands, there is a difference in the number of rotatable bonds that can be possibly immobilized upon binding to the protein. For instance, in Autodock the entropic penalty is assigned a default value of 0.31 kcal/mol per bond. The calculated $\Delta\Delta G°$ in Figure 7 takes this contribution into account when deemed present, i.e., when the ligands to be compared differ in the number of potentially immobilized rotatable bonds. The lines extending inward or outward of the calculated $\Delta\Delta G°$ bar values show the results obtained by neglecting the entropic penalty. It is apparent that the general trend is maintained whether or not such contribution is taken into account. Solvent effects due to the variations of interface

(45) Hu, X.; Balaz, S.; Shelver, W. H. *J. Mol. Graph. Model.* **2004**, *22*, 293−307.

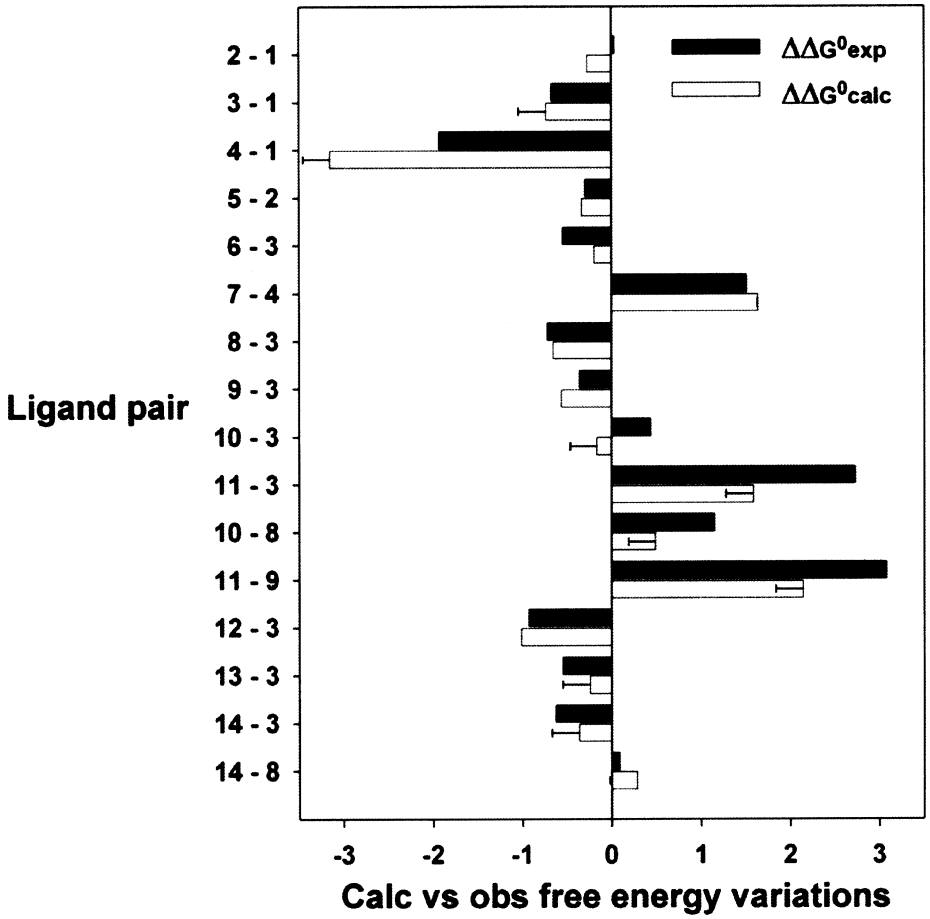


***Figure 7.*** Calculated (white bars) and observed (black bars) free energy variations ($\Delta\Delta G°$) on passing from one MMP12 adduct to another with a close analogue ligand. The calculated $\Delta\Delta G°$ values are the algebraic sum of all the intermolecular interaction energies plus a entropic penalty term related to immobilization of rotatable bonds as described in Materials and Methods. The lines extending inward or outward of the calculated $\Delta\Delta G°$ bar values show the results obtained by neglecting the entropic penalty. The individual intermolecular interaction energy differences are illustrated in Figure 2 for ligand pairs **2-1**, **3-1**, and **4-1**, in Figure 3 for ligand pairs **5-2**, **6-3**, and **7-4**, in Figure 4 for ligand pairs **8-3**, **9-3**, **10-3**, and **11-3**, in Figure 5 for ligand pairs **10-8** and **11-9**, and in Figure 6 for ligand pairs **12-3**, **13-3**, **14-3**, and **14-8**.

areas buried in the protein−ligand interface also contribute to the energetics. In other approaches these effects are explicitly taken into account. In the Autodock parametrization, solvent effects are taken into account implicitly.

In our opinion, the results in Figure 7 constitute a strong validation of the use of energetic considerations to examine the details of the structure−affinity relationships in this series of homologous MMP inhibitors. We turn now to describe such details, to further show that their information content is adequate to make this approach vital in terms of predictive power for the refinement of inhibitors toward a particular target.

**$R_1$ Groups.** The first three pairs of experimental $\Delta\Delta G°$ values in Figure 7 show that the substitution of a hydrogen atom in para position to the phenyl substituent targeted to the hydrophobic $S_{1'}$ pocket with -F (**2**), -$OCH_3$ (**3**), or a -$C_6H_5$ (**4**) $R_1$ group is essentially neutral, moderately advantageous, and strongly advantageous, respectively. The corresponding estimated $\Delta\Delta G°$ values (Figure 7) agree very well with the observations, albeit with a slight tendency to overestimate the improvement. From Figure 2A−C it appears that the atoms involved in improving the binding are mostly the additional atoms in the $R_1$ group, as expected. The rest of the molecular scaffold is scarcely affected. However, it is interesting to notice that the perturbations on the rest of the scaffold are larger in the -$OCH_3$ than in the -F derivative, and that they extend as far as to affect the coordination of the hydroxamic group to the zinc ion. It is also interesting to note that individual interactions can both gain and lose strength, with a prevalence of the latter. This is to be expected as the bulkier the $R_1$ group, the fewer the degrees of freedom available to the rest of the molecule to optimize these individual interactions. The worsening of a subset of other interactions in the rest of the molecule is particularly apparent for $R_1$ = -$C_6H_5$: its presence does substantially increase the total hydrophobic interactions in the $S_1'$ pocket but at the same time decreases the hydrophobic interactions of the first phenyl ring (right-hand side of Figure 2C). As noticed already by comparing the left and central panels in Figure 2C, the presence of the second ring apparently prevents the first phenyl ring from entering the $S_1'$ pocket as deeply as in the unsubstituted derivative. Also the other qualitative observations made by comparing the structures in panels A−C in Figure 2 are confirmed: -F introduces the least perturbations, slightly worsening the hydrophobic interactions in the $S_1'$ pocket and the hydrogen bonds of the $SO_2$ group, while in the -$OCH_3$ derivative an appreciable worsening is transmitted to the hydroxamic moiety, and in the -$C_6H_5$ derivative there is a modest but clear decrease of the hydrophobic interactions of the first phenyl ring with the $S_1'$ pocket.

**$R_2$ = -$CH_2CH_2OH$.** For three derivatives with $R_1$ = -F (**5**), -$OCH_3$ (**6**), and -$C_6H_5$ (**7**), the effect of substituting the hydrogen

atom in position $R_2$ with -$CH_2CH_2OH$ was investigated. The alcoholic substituent in $R_2$ slightly improves the binding to the enzyme for the first two derivatives and sizably worsens the binding for the third. Again, the estimated $\Delta\Delta G°$ values agree very well with the observations (Figure 7). Panels A−C in Figure 3 provide a rationale for the different behavior. In summary, in all three cases the $R_2$ substituent provides an appreciable contribution to binding, especially through hydrophobic interactions of the two additional $CH_2$ groups. For $R_1$ = -F this is accompanied by a modest worsening of the hydroxamic coordination strength. Conversely, for $R_1$ = -$OCH_3$ the hydroxamic coordination is actually slightly improved, and a modest worsening of the hydrophobic contact of the phenyl ring is seen. Thus, in no case a perfect fit is achieved. It is interesting to note that the nonperfect fits for the two different molecules lead to different compromises for the interactions with the three enzyme subsites: For $R_1$ = -F, the interaction is optimized for the hydrophobic pocket and the substrate binding groove, while the binding to zinc is sacrificed. For $R_1$ = -$OCH_3$ the interaction is optimized for the binding to zinc and to the substrate binding groove, while the binding to the hydrophobic pocket is sacrificed.

Unexpectedly, the $R_2$ = -$CH_2CH_2OH$ substitution has a sizable destabilizing effect on the $R_1$ = -$C_6H_5$ scaffold. In this case, the binding to zinc is strongly worsened, and the additional interactions established by the alcoholic $R_2$ group do not compensate for the loss of interaction strength of the zinc-binding group. Apparently, a sizable steric misfit is being faced in this derivative. Figure 2C shows that there is almost no perturbation of the hydrophobic interactions of the biphenyl group with respect to those experienced by the same group in the $R_2$ = -H derivative. This suggests that the two phenyl rings together are held so tightly in the $S_1'$ pocket that the steric perturbation introduced by the $R_2$ substituent on the sulfonamide nitrogen, which is apparently tolerated in the $R_1$ = -F and $R_1$ = -$OCH_3$ derivatives, is not tolerated by the $R_1$ = -$C_6H_5$ derivative. As a consequence, a serious mismatch of the hydroxamic moiety in the zinc subsite occurs. It should be recalled that the hydroxamic group, if free to optimize its orientation, is very specifically tailored for the MMP active site, featuring bidentate binding to zinc together with two strong hydrogen bonds, one with the carboxylate side chain of the active site Glu-219 and one with the peptide carbonyl group of Ala-182.

**$R_3$ = -D,L-Ser or -D,L-Thr.** The effect of these substituents (**8**−**11**) has been examined on the scaffold having $R_1$ = -$OCH_3$. The D stereoisomers have higher affinity, and the L stereoisomers lower affinity, for MMP12 with respect to the $R_3$ = -H scaffold (Figure 7). Examination of Figure 4A−D again provides a full rationale for this behavior: The D-isomers, besides providing additional binding interactions with the $R_3$ group, also exert a slight stabilizing effect on the hydroxamic moiety. The stabilization is somewhat larger for the D-Thr derivative but is accompanied by a modest weakening of the sulfonamide nitrogen interactions, so that the overall gain in affinity is slightly lower for the D-Thr (**9**) than for the D-Ser (**8**) derivative. In the L-Ser stereoisomer (**10**) the stabilizing effect on the hydroxamic moiety is estimated to be essentially lost, leading to a very small overall stabilization effect, while the experimental $\Delta\Delta G°$ indicates an overall modest destabilization. Finally, the behavior of the $R_3$ = L-Thr (**11**) is strikingly different, both the experiment and the computational estimate showing a strong destabilization. Figure 5A,B shows that the L-Thr group actually has slightly more stabilizing interactions that the D-Thr group; however, its stereochemistry causes an appreciable distortion of the scaffold that apparently strongly destabilizes *both* the hydroxamic moiety and the sulfonamide NH and $SO_2$ groups. Again, it is remarkable that the experimental $\Delta\Delta G°$ trend is reproduced so well by these simple calculations (Figure 7).

Figure 7 also shows the direct differences between the L and D isomers and confirms the analysis. In the case of the Ser derivatives (**8**, **10**) the L isomer slightly stabilizes the Ser itself and mainly destabilizes the hydroxamic moiety, while in the case of the Thr derivatives (**9**, **11**) the Thr itself is slightly stabilized, but the hydroxamic moiety and the sulfonamide NH and $SO_2$ groups are substantially destabilized. This direct comparison between the L and D isomers is of course redundant, because the effects could have been deduced from the preceding panels of Figure 7. However, it is instructive because the $\Delta\Delta G°$ values in this latter comparison are by definition free from solvent−ligand interactions and essentially free also from solvent−protein interactions. In other words, the $\Delta\Delta G°$ values almost purely reflect ligand−protein interactions.

**$R_2$ = -$CH_2CH(CH_3)_2$; $R_2$ = -$CH_2CHOHCH_2OH$ with $R_3$ ≡ -H, -$CH_2OH$.** Having established that the -$OCH_3$ substitution in $R_1$ allows substituents in either $R_2$ or $R_3$ to increase the overall affinity for MMP12, the relative effects of hydrophobic vs hydrophilic substituents in $R_2$ was investigated for $R_1$ = -$OCH_3$, both in the absence (-H) or in the presence (-$CH_2OH$) of a substituent in $R_3$ with a D configuration. The experimental and predicted $\Delta\Delta G°$ values for hydrophobic (**12**) vs hydrophilic (**13**) $R_2$ are shown in Figure 7, and the calculated energetics of the individual interactions are reported in Figure 6A−D. The estimated sign of the effect is again correct, i.e., both $R_2$ groups are predicted and found to stabilize the $R_1$ = -$OCH_3$, $R_2$ = -H, $R_3$ = -H scaffold, although the stabilizing effect is somewhat overestimated for the hydrophobic substituent and underestimated for the hydrophilic substituent. In the first case, Figure 6A shows that the hydrophobic substituent has by itself a strong stabilizing effect, on top of which a non-negligible stabilization of the hydroxamic moiety is also observed. In the second case (Figure 6B), the stabilizing effect of the $R_2$ substituent is smaller, but the stabilizing effect on the hydroxamic moiety is maintained. These findings are consistent with what observed for the $R_2$ = -$CH_2CH_2OH$ case already discussed: it can be concluded that for $R_1$ = -$OCH_3$ (but not $R_1$ = -F or $R_1$ = -$C_6H_5$) any substituent at $R_2$ improves the binding of the hydroxamic group. With this in mind, the derivative with $R_2$ = -$CH_2$-$CHOHCH_2OH$ and $R_3$ = -$CH_2OH$ simultaneously present (**14**) was tested. These $R_2$ and $R_3$ groups, taken separately, both improved the binding of the starting $R_1$ = -$OCH_3$ scaffold. Figure 7 shows that the effect is not synergistic, the improvement being of the same order of each substituent separately, and actually slightly smaller than that caused by the $R_3$ = -$CH_2OH$ substituent alone. Again, the calculations are in qualitative agreement in all cases. Figure 6C,D surprisingly shows that the hydroxamic moiety and the $SO_2$ groups are both improved by the simultaneous presence of the two substituents, but each substituent adopts a less optimal set of interactions with the protein, essentially neutralizing the improvement.

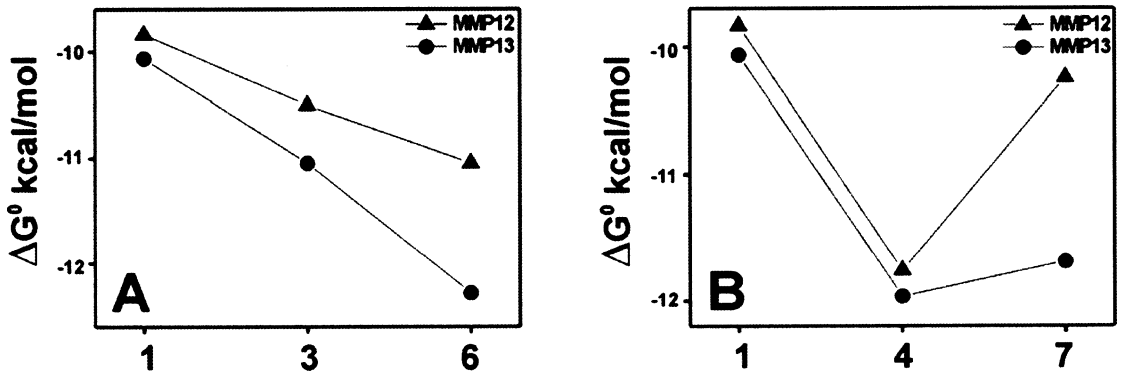


***Figure 8.*** Experimental free energy of binding to MMP12 (up triangles) and MMP13 (filled circles) for ligands **1**, **3**, and **6** (A) and **1**, **4**, and **7** (B). The increased discrimination between MMP12 and MMP13 is highlighted.

**Implications for Drug-Design Strategies.** The above analysis demonstrates that the availability of high-resolution structures of a series of enzyme adducts with homologous ligands provides precious information on the subtle factors that modulate ligand affinity and thus may be of much help in the optimization of such ligands. For instance, increasing the size of the hydrophobic group in the $S_1'$ pocket increases the affinity but only provided that no substituents are placed in $R_2$ and $R_3$ positions. Conversely, a smaller hydrophobic group such as the one with $R_1 = -OCH_3$ permits the insertion of other groups, including more hydrophilic groups, in $R_2$ and $R_3$, provided their local effect is not destabilizing. One could even conceive substitutions in $R_1$, $R_2$, and $R_3$ that strongly destabilize the hydroxamic moiety but provide enough local stabilization to partially compensate for the loss. Under such circumstances, the substitution of the now unfit hydroxamic moiety with a more druggable group with a better fit could provide enough extra stabilization to obtain nanomolar affinity for a non-hydroxamic ligand. For example, we predict that a non-hydroxamic ligand could provide a reasonable binding affinity in the case of **7**, which displays a nonoptimal fit of the hydroxamic moiety (Figure 3). Regarding the $R_2$ and $R_3$ substituents, the present results also show that hydrophilic substitutions are not severely disfavored with respect to hydrophobic substitutions, as commonly assumed for this class of molecules. Furthermore, as other MMPs such as MMP13 have a larger binding site, one could exploit the present findings to test ligands with substituents in, e.g., $R_1$, $R_2$, that show more or less pronounced steric misfit in MMP12 for improved selectivity for MMP13. Indeed, $\Delta G°$ data on binding of selected ligands to MMP13 confirm the correctness of the approach (Figure 8): adding an $R_2 = CH_2CH_2OH$ to the $R_1 = OCH_3$ or $R_1 = C_6H_5$ scaffolds stabilizes the adduct with MMP13 more, or destabilizes it less, than the corresponding adduct with MMP12, resulting in both cases in an increased selectivity for MMP13. Of course, if suitable crystals for ligand soaking were available for other MMPs, the potential of this strategy would be further enhanced. Finally, the degree of prediction achieved with the present strategy should help avoiding the extensive screening of substituents in *n* different positions ($R_1$, $R_2$, and $R_3$ in this case) by examining a full *n*-dimensional matrix of compounds. Indeed, once the interplay among a certain set of substituents shows that one position is disfavored, examining further substitutions in that position with the chosen set of substituents can be avoided.

It should be stressed that the above findings have only been made possible by the availability of experimental structures. While docking programs are able to provide reasonable models of ligand binding modes, especially in the presence of existing structures with homologous ligands, the accuracy of the resulting models is lower than that of experimental structures, and insufficient for the present purpose. This has been tested by taking the high-resolution (1.1 Å) crystal structure of MMP12 and using it to dock all the inhibitors described in this work. Despite the overall binding mode always being correct, the details of the interatomic distances were not accurate enough to make any energetic predictions. One drawback is the use of the same protein structure for all adducts, while the present work shows that the protein structures differ slightly from one another in the various adducts, as a consequence of some mutual adaptation or "induced fit". Attempts to mimic this induced fit, either by allowing protein side-chain movements during docking or by overall (i.e., ligand and protein) restrained energy minimization of the final adduct did not improve the energetic predictions significantly (data not shown). On the other hand, it is reassuring that the choice of the set of potentials to extract energetic information from the experimental structures is not critical, as different popular potential sets provide similar results.

**Thermodynamics of Ligand Binding.** Of course, it is well-known that the relationship between $\Delta G°$ and intermolecular potential energy calculations is totally empirical, although it is often found to hold.[46−48] There are two reasons to question its applicability. The first reason is that contributions to $\Delta G°$ from solvent−ligand, solvent−protein, and solvent−adduct interactions are not taken into account. However, it can be speculated that, at least in systems of this kind, solvation effects are not so strong, and there is always partial cancellation between solvent effects on the reactants and the product. Furthermore, in our approach $\Delta\Delta G°$ values are estimated, so the differential solvent−protein effects are zero, and the other two terms are likely to be further reduced. In one case, i.e., the comparison between the behavior of the D- and L- isomers substituted in $R_2$, solvent effects on the ligands are also zero, and the differential solvent-adduct effects are probably negligibly small. It is obvious that the striking difference in binding affinity

(46) Lamb, M. L.; Jorgensen, W. L. *Curr. Opin. Chem. Biol.* **1997**, *1*, 449−457.
(47) Aqvist, J.; Luzhkov, V. B.; Brandsdal, B. O. *Acc. Chem. Res.* **2002**, *35*, 358−365.
(48) Osterberg, F.; Morris, G. M.; Sanner, M. F.; Olson, A. J.; Goodsell, D. S. *Proteins Struct. Funct. Genet.* **2002**, *46*, 34−40.

between the $R_2$= D-Thr and $R_2$ = L-Thr is almost entirely due to the difference in protein−ligand interaction.

The second reason is that, even if the leading term is the free energy of the protein−ligand interaction, the latter is still composed by enthalpic and entropic terms, and intermolecular interaction energy calculations only take into account the enthalpic term (except for a modest correction for possible differences in number of immobilized rotatable bonds). Prompted by these considerations, $\Delta H°$ values for the binding of some of the present ligands were measured through isothermal titration calorimetry (ITC). Two other well-known strong MMP ligands, actinonin and galardin (Biomol Inc.), were also studied for comparison purposes.

**ITC Measurements.** Isothermal titration calorimetry is widely used in drug discovery, since it permits an accurate and extensive thermodynamic characterization of protein−ligand interactions.[49,50] In particular, ITC measurements have already been successfully exploited to design and characterize Stromelysin inhibitors.[51,52]

All measurements were performed at 298 K. At variance with fluorimetric assays, here the protein concentrations were much higher (20 $\mu$M), and the AHA concentration was correspondingly higher (4 mM). This concentration is comparable with the dissociation constant of AHA itself. Therefore, AHA interferes with the binding of the inhibitors, and the experimental $\Delta H°$ values are conditional values. A proper estimate of the $\Delta H°$ for AHA was needed, both to obtain the true $\Delta H°$ values for the other inhibitors and to obtain thermodynamic parameters of AHA itself. A series of ITC measurements on the binding of the **3** ($R_1$ = $OCH_3$, $R_2$ = H) were thus performed in the presence of various AHA concentrations in the range 1 to 256 mM. By fitting the obtained enthalpy as a function of AHA concentration, a $\Delta H°$ of −3.180 kcal/mol was found for the binding of AHA. The latter parameter provides an experimental estimate of the enthalpic contribution of the metal binding group to the overall binding of all the inhibitors investigated here, as well as of all hydroxamic-based inhibitors in general, to MMP12. Furthermore, the AHA $\Delta H°$ value allowed us to estimate the correction to apply to the other $\Delta H°$ values. The corrected thermodynamic parameters of some of the inhibitors investigated here, as well as those of AHA, are reported in Table 1.

Although ITC measurements performed at increasing inhibitor concentrations as in the present experimental scheme also provide estimates of the dissociation constants, the latter are affected by large errors when the constants approach nanomolar values, and so are the derived $\Delta G°$ values. Conversely, the $\Delta H°$ values are not affected by such errors. Therefore, estimates of $-T\Delta S°$ values were obtained by using the corrected $\Delta H°$ values from calorimetry and the $\Delta G°$ values from fluorimetry measurements. The $-T\Delta S°$ values are also reported in Table 1. The binding constants derived from ITC measurements (not shown) were in any case within a factor two with respect to the fluorimetric values.

From the $\Delta H°$ and $-T\Delta S°$ values reported in Table 1 it appears that the free energy of binding of all the homologous ligands examined in this work contain an important enthalpic contribution and a less important but sizable entropic contribution, both favorable to binding. This appears a general feature for this class of ligands but is by no means general for other inhibitors of MMPs. For instance, galardin and actinonin, two well-known strong inhibitors of MMPs, show much less favorable, or even unfavorable, enthalpic contributions, respectively, and much more favorable entropic terms (Table 1).

By examination of the $\Delta H°$ values in Table 1, no apparent correlation can be seen with the corresponding $\Delta G°$ values, neither with the intermolecular interaction energies estimated from the experimental structures in the present homologous series of ligands; nor do the differences $\Delta\Delta H°$ correlate better with the $\Delta\Delta G°$. Apparently, the enthalpies (and entropies) of the ligand−solvent interactions are sizable and vary in a rather unpredictable way, while they largely cancel each other to give a modest contribution to $\Delta G°$. Apparently, this is yet another manifestation of the well-known entropy−enthalpy cancelation phenomenon.

An interesting finding from ITC measurements is the fact that, as already observed for stromelysin,[52] the binding of AHA to MMP12 (and thus presumably to all others MMPs) is almost exclusively enthalpy-driven. The $\Delta H°$ value of about −3.2 kcal/mol for this ligand having millimolar affinity is only two to three times smaller than the binding enthalpy of nanomolar affinity ligands, which is a relevant contribution. The $-T\Delta S$ value for AHA is close to zero. This relatively strong contribution to the overall binding enthalpy could be even higher if the ligand solvent contribution were not unfavorable, as it is expected to be for the very soluble AHA molecule. Indeed, in our parametrization, the estimated contribution of the AHA moiety to the overall protein−ligand interaction energy has to be as high as −6 kcal/mol if a reasonable estimate of the overall interaction energy for this class of ligands has to be obtained. This is not unexpected, as it is well-known that, if AHA is considered a fragment of a strong binding ligand rather than an independent molecule, the loss of rigid body rotational and traslational entropy upon binding occurs only once and not twice as it would be for the isolated fragments. The corresponding gain in $\Delta G°$, which is parametrically incorporated in the interaction energy in our calculations, can easily be of the order of −3 kcal/ mol.[52−54]

## Conclusion

In summary, it is shown here that an analysis of the details of the protein−ligand interactions, as they appear from the three-dimensional structures in terms of simple hydrophobic and electrostatic contributions, provides a remarkable semiquantitative account of (i) the $\Delta G°$ values of the adducts, (ii) the differences in $\Delta G°$ ($\Delta\Delta G°$) between pairs of closely related ligands, and (iii) the identity of the individual ligand atom−protein atom interactions that contribute in each case to increase, or decrease, the affinity of each particular ligand with respect to its closest analogue. This work demonstrates that this kind of rationalization is possible and reliable and provides hints for

(49) Holdgate, G.; Fisher, S.; Ward, W. The Application of Isothermal Titration Calorimetry to Drug Discovery. In *Biocalorimetry 2*; Ladbury, J. E., Doyle, M. L., Eds.; John Wiley & Sons Ltd: Chichester, 2004.
(50) Ruben, A. J.; Kiso, Y.; Freire, E. *Chem. Biol. Drug Des.* **2006**, *67*, 2−4.
(51) Parker, M. H.; Lunney, E. A.; Ortwine, D. F.; Pavlovsky, A. G.; Humblet, C.; Brouillette, C. G. *Biochemistry* **1999**, *38*, 13592−13601.
(52) Olejniczak, E. T.; Hajduk, P. J.; Marcotte, P. A.; Nettesheim, D. G.; Meadows, R. P.; Edalji, R.; Holzman, T. F.; Fesik, S. W. *J. Am. Chem. Soc.* **1997**, *119*, 5828−5832.
(53) Jencks, W. P. *Proc. Natl. Acad. Sci. U.S.A.* **1981**, *78*, 4046−4050.
(54) Murray, C. W.; Verdonk, M. L. *J. Comput.-Aided Mol. Des.* **2002**, *16*, 741−753.

the planning of finely tuned inhibitors, originating from the same scaffold, for any structurally well-characterized biological target.

For some of the present ligands, the enthalpies of binding ($\Delta H°$) were also measured through isothermal calorimetry. All the ligands from this class are found to be characterized by favorable enthalpic as well as entropic contributions. The enthalpic contribution of the hydroxamic moiety, a popular zinc-binding group in the MMP inhibitor landscape, has been separately evaluated and discussed in terms of its relative contribution to the potency of hydroxamic-based MMP ligands. A detailed analysis of the $\Delta H°$ and $\Delta S°$ values, taken separately, is less instructive, due to the well-known entropy−enthalpy compensation effects.[49] As in many other thermodynamic studies, the two terms are found to provide opposite and largely canceling contributions to $\Delta G°$.

**Acknowledgment.** This work was supported by EC (Projects: LSHG-CT-2004-512077and TOC: MTKI-CT-2004-509750), MIUR (PRIN 2005, Prot. N. 2005039878, Prot. N. 4455, and RBAU013NSB), and Ente Cassa di Risparmio di Firenze (Innovative Strategies for Drug Design).

**Supporting Information Available:** Data collection, processing statistics, and refinement statistics for all crystallographic datasets; full references 6 and 7. This material is available free of charge via the Internet at http://pubs.acs.org.

JA065156Z